Real-space magnetic imaging of the multiferroic spinels MnV_2O_4 and Mn_3O_4

B. Wolin,[1] X. Wang,[1] T. Naibert,[1] S. L. Gleason,[1] G. J. MacDougall,[1] H. D. Zhou,[2,3] S. L. Cooper,[1] and R. Budakian[1,4,5,6,7]

[1]Department of Physics and Frederick Seitz Materials Research Laboratory, University of Illinois, Urbana, Illinois 61801, USA
[2]Department of Physics and Astronomy, University of Tennessee, Knoxville, Tennessee 37996-1200, USA
[3]National High Magnetic Field Laboratory, Florida State University, Tallahassee, Florida 32310-3706, USA
[4]Department of Physics, University of Waterloo, Waterloo, Ontario, Canada, N2L3G1
[5]Institute for Quantum Computing, University of Waterloo, Waterloo, Ontario, Canada, N2L3G1
[6]Perimeter Institute for Theoretical Physics, Waterloo, Ontario, Canada, N2L2Y5
[7]Canadian Institute for Advanced Research, Toronto, Ontario, Canada M5G1Z8

(Received 5 April 2018; published 22 June 2018)

Controlling multiferroic behavior in materials will enable the development of a wide variety of technological applications. However, the exact mechanisms driving multiferroic behavior are not well understood in most materials. Two such materials are the spinels MnV_2O_4 and Mn_3O_4, where mechanical strain is thought to play a role in determining magnetic behavior. Bulk studies of MnV_2O_4 have yielded conflicting and inconclusive results, due in part to the presence of mesoscale magnetic inhomogeneity, which complicates the interpretation of bulk measurements. To study the sub-micrometer-scale magnetic properties of Mn-based spinel materials, we performed magnetic force microscopy (MFM) on MnV_2O_4 samples subject to different levels of mechanical strain. We also used a crystal grain mapping technique to perform spatially registered MFM on Mn_3O_4. These local investigations revealed 100-nm-scale "stripe" modulations in the magnetic structure of both materials. In MnV_2O_4, the magnetization of these stripes is estimated to be $M_z \sim 10^5$ A/m, which is on the order of the saturation magnetization reported previously. Cooling in a strong magnetic field eliminated the stripe patterning only in the low-strain sample of MnV_2O_4. The discovery of nanoscale magnetostructural inhomogeneity that is highly susceptible to magnetic field control in these materials necessitates both a revision of theoretical proposals and a reinterpretation of experimental data regarding the low-temperature phases and magnetic-field-tunable properties of these Mn-based spinels.

DOI: 10.1103/PhysRevMaterials.2.064407

I. INTRODUCTION

The wide variety of interactions and degrees of freedom in condensed matter systems yield some of the most complex and challenging problems in physics. When different types of order compete, materials can exhibit rich phase diagrams with linked structural, magnetic, and orbital ordering transitions. Two phenomena of great interest can result from this competition: multiferroism—the coexistence and coupling of different types of ferroic order (ferromagnetism, ferroelectricity, and ferroelasticity)—and magnetoresponsive behavior, i.e., large susceptibilities of physical properties to external perturbations, such as applied magnetic fields and pressure. Magnetoresponsive and multiferroic materials show great promise for practical applications, ranging from high-frequency actuators to precision sensors [1].

Various mechanisms can cause a coupling between magnetic and other primary order parameters [2–4], including the development of noncollinear spin order that breaks inversion symmetry [2,3], and the formation of multiferroic domains [4,5] and domain walls [6,7]. One of the grand challenges in the study of multiferroic and other magnetoresponsive materials has been to identify the specific magnetostructural and magnetoelectric mechanisms responsible for the different magnetoresponsive phenomena observed in numerous complex magnetic materials, including $ACuO_3$ ($A =$ Se,Te) [8], Mn-doped $BiFeO_3$ [9], $EuTiO_3$ [10], $Y_2Cu_2O_5$ [11], $YbMnO_3$ [12], and the spinels $CoCr_2O_4$ [5], $MnCr_2O_4$ [13], MnV_2O_4 [14,15], and Mn_3O_4 [16–19].

The magnetic spinel family of compounds (chemical formula AB_2X_4)—which consists of an A-site diamond sublattice and a geometrically frustrated B-site pyrochlore sublattice [20]—is a particularly promising class of materials for studying the microscopic origins of magnetoresponsive behavior in magnetic materials. Magnetic spinels exhibit a range of diverse phases and phenomena that can be sensitively tuned using a variety of methods, including A- and/or B-site substitution, applied pressure, and/or applied magnetic field [5,13–19,21]. Due to the strong sensitivity of their physical properties to pressure and magnetic field, the magnetic spinels have important potential applications in catalysis, electrochemistry, and magnetic shape memory [22–27]. More broadly, magnetic domain formation is known to play a key role in raising the susceptibilities of complex materials to external perturbations [6,7,28,29]. However, the potential role of this mesoscale inhomogeneity on the magnetoresponsive properties of spinels has not been well investigated, because most previous research on the spinels has been conducted using bulk probes focusing on atomic length scales such as neutron scattering [30–32], SQUID magnetometry [33–35], x-ray diffraction [33,36,37], and Raman scattering [38,39].

In this report, we explore the role of 0.1–10 μm scale magnetic inhomogeneity on the magnetic properties of two specific spinels, MnV_2O_4 and Mn_3O_4, using magnetic force microscopy (MFM). By using a sub-micrometer-size magnetic probe, MFM can measure magnetic properties that are averaged over just tens of unit cells. Consequently, MFM measurements can reveal small-scale (0.1–100 μm) magnetic inhomogeneities that have been overlooked in bulk measurements. We select the Mn-based magnetic spinels, MnV_2O_4 and Mn_3O_4, for study, because both materials exhibit similar magnetostructural properties and transitions at cryogenic temperatures that depend sensitively on the *B*-site constituent, V or Mn. For example, MnV_2O_4 is a cubic paramagnet at room temperature, and undergoes a magnetic transition to a collinear ferrimagnetic (FEM) configuration below $T = 57$ K. A second transition to a Yafet-Kittel (YK) type FEM configuration accompanied by a cubic-to-tetragonal structural transition occurs at $T = 53$ K [30,33,36,40]. By contrast, the cubic-to-tetragonal structural transition in Mn_3O_4 occurs at a significantly higher temperature, $T = 1440$ K, and the low-temperature magnetostructural phase behavior is more complex: Mn_3O_4 is a tetragonal paramagnet at room temperature and develops a triangular FEM configuration near $T = 42$ K. Near $T = 39$ K, an incommensurate spin ordering develops before Mn_3O_4 finally transitions to a cell-doubled YK-FEM magnetic phase with an orthorhombic crystal structure near $T = 33$ K [30–32,41].

In this study, we collected MFM images across a wide range of temperatures and magnetic fields from two samples of MnV_2O_4 with different levels of induced mechanical strain. We also studied MFM images from a single sample of Mn_3O_4 with inherent strain produced during crystal growth. Among a diverse range of magnetic patterns, we observe 100-nm scale "stripe" modulations in the magnetic structure present in the lowest-field phases of both materials. These stripe modulations are further organized into 1–10 μm scale domains associated with the local crystal structure. In Mn_3O_4, an observed correlation between stripe width and encompassing tetragonal domain size evidences a connection between mechanical strain and the magnetic patterns. In MnV_2O_4, we observe 100-nm-scale stripe modulations consistent with recent zero-magnetic-field TEM measurements of thin-foil MnV_2O_4 [42], and we find different magnetic behaviors in the high- and low-strain MnV_2O_4 samples. We also present a quantitative estimate of the local magnetization associated with these stripe domains in MnV_2O_4. We observe that modest applied magnetic fields (<30 kG) cause dramatic changes to—and the ultimate elimination of—the stripe domain patterns in both Mn_3O_4 and low-strain MnV_2O_4, but not in high-strain MnV_2O_4. These findings are consistent with theoretical results showing that mesoscale magnetic inhomogeneity can significantly lower the energy barrier for strain- and field-dependent phase changes in complex materials [28,29], and suggests that magnetic domain formation plays an important role in the magnetoresponsive behavior of these spinel materials.

II. METHODS

Single crystals of MnV_2O_4 were grown at the National High Magnetic Field Laboratory in Tallahassee using a traveling-solvent-floating-zone technique. Mixtures of MnO and V_2O_3 were ground, pressed, and calcined to form the seed and feed rods. A greater than stoichiometric amount of V_2O_3 was used to compensate for evaporation during growth. Details of the growth and characterization are reported elsewhere [33]. Single crystals of Mn_3O_4 were grown at the University of Illinois using a floating-zone technique. Commercially available Mn_3O_4 powder was pressed and sintered to form the feed and seed rods. The structural and magnetic properties of the resulting crystals are also reported elsewhere [16,41]. For both materials, crystallographic orientations were determined via room-temperature x-ray diffraction.

After characterization, the crystal surface normal to the [001] (cubic) direction was polished to <50 nm roughness, and sputter coated with a 5-nm layer of Au-Pd to dissipate static charge. Two MnV_2O_4 samples were prepared from the same growth. The first sample was a half-boule semicylinder measuring approximately 5 mm × 2.5 mm × 0.5 mm. Epoxy was applied to the entire back surface of this sample, which was then attached to a sapphire backing-plate. The total thermal contraction occurring between the epoxy curing temperature and the base temperature used in this study ($T = 4$ K) is ten times larger for the epoxy than for the MnV_2O_4, and therefore significant mechanical strain is induced in the sample below $T = 77$ K [42]. A similar order-of-magnitude difference in thermal expansion coefficients between MnV_2O_4 foil and the Mo mount resulted in an estimated 0.03% compressive strain in MnV_2O_4 at 87 K and a <0.1% compressive strain near the cubic-to-tetragonal transition at 52 K in MnV_2O_4 [42]. While this estimated compressive strain is less than the ∼0.15% lattice striction measured in MnV_2O_4 at the cubic-to-tetragonal transition [37], it is large enough to influence domain formation in MnV_2O_4 [42]. The second MnV_2O_4 sample was a full-boule cylinder having a 5 mm diameter and a 2 mm length, and was specifically prepared to minimize mechanical strain below $T = 77$ K. This sample was attached to a copper backing plate using a single point of epoxy at one edge, allowing the sample to thermally contract without interference from either the epoxy or backing plate. The increased sample thickness and single epoxy point mounting both act to minimize mechanical strain at the sample surface. Thermal contact between the sample and backing plate was maintained through the epoxy and physically through the sample-plate interface. In addition, long soak times (∼10 minutes) were used to ensure thermal equilibrium was achieved.

Single crystals of Mn_3O_4 were grown at the University of Illinois using a traveling-solvent-floating-zone technique. To prepare the Mn_3O_4 sample, the Mn_3O_4 rod was diced into a rectangular block measuring approximately 1 mm × 2 mm × 1 mm. The sample was polished normal to the [110] (tetragonal) direction and sputter coated with 1nm Au-Pd to prevent charging. The Mn_3O_4 sample was lithographically patterned with an array of unique location markers to provide spatial location information. We performed cryogenic electron backscatter diffraction (EBSD) experiments to determine the tetragonal crystal grain structure for comparison to MFM measurements. Using the location markers, we were able to align the magnetic and crystallographic data images with approximately 50 nm accuracy, allowing us to correlate observed magnetic phenomena with the local crystal domain structure.

We performed low-temperature, frequency-modulated MFM using a ^{4}He bath cryostat that had a built-in supercon-

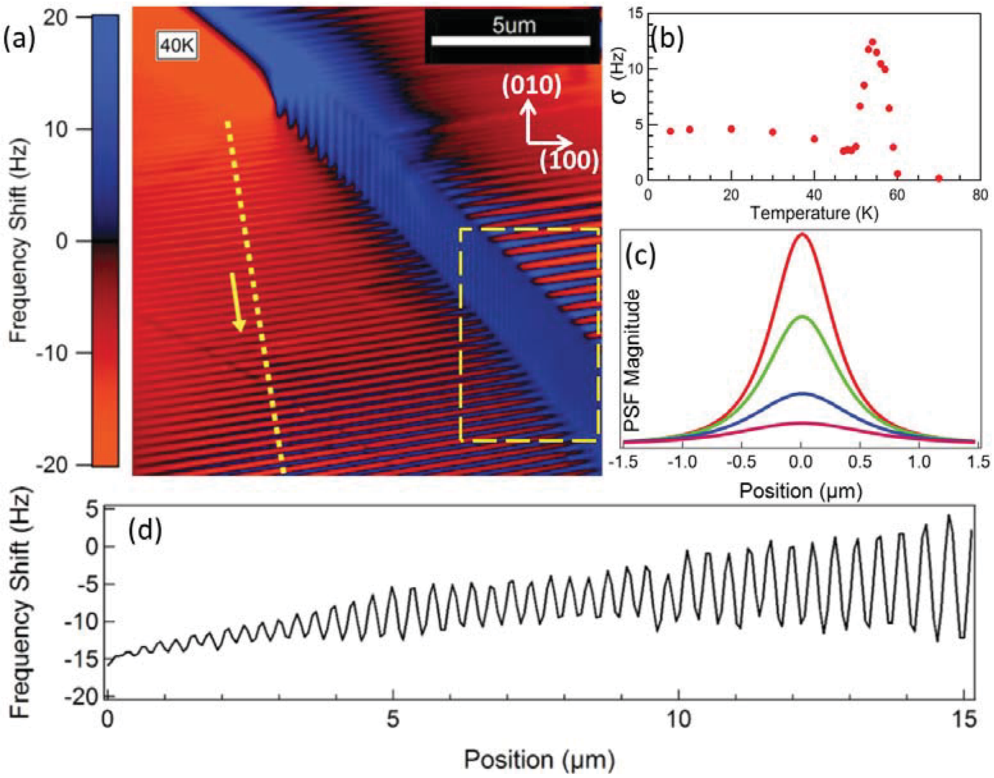

FIG. 1. MFM data of high-strain MnV_2O_4 cooled from 70 to 40 K in $B = 0.3$ T. (a) When cooled in a weak magnetic field, the magnetic pattern sharpens dramatically. We observe 20-μm-scale domain structure with regular subdomain stripe modulations. Regions of overall frequency shift (predominant blue or red color) correspond to areas of a single stripe direction. Approximate cubic lattice axes are indicated in white. The yellow dashed box highlights a region where mechanical strain influences the magnetic pattern. (b) Average magnitude of magnetic inhomogeneity (characterized by the standard deviation of frequency shift) measured while cooling the high-strain MnV_2O_4 sample in zero magnetic field. Note the qualitative similarity to measurements of the bulk sample magnetization. (c) Cross sections of the measured point spread function at locations: (top to bottom) 0, 250, 500, and 750 nm away from the PSF center. (d) Frequency data along the indicated line through the 2D image. Stripe pitch, frequency offset, and amplitude vary across the domain.

ducting magnet. Data were collected in the temperature range from $T = 4.5$ to 80 K and the magnetic field range from $B = 0$ to 3 T. In all cases, the magnetic field was oriented normal to the sample surface, resulting in B parallel to [001] (cubic) for both MnV_2O_4 samples and B parallel to [110] (tetragonal) for the Mn_3O_4 sample. Commercially available atomic force microscopy cantilevers were evaporatively coated with a 10-nm-thick layer of FeCo to provide magnetic sensitivity. With probe-sample separations of approximately 100 nm and scan rates as low as 100 nm/s, we were able to achieve a spatial resolution of approximately 50 nm for magnetic features. The cantilevers used in these experiments have resonance frequencies approximately $f_0 \sim 25$ kHz, spring constants approximately $k \sim 0.3\,\mathrm{N/m}$, and quality factors approximately $Q \sim 350\,000$ at $T = 4$ K in vacuum. We measured the cantilever displacement interferometrically using a 1510-nm laser in a fiber-optic Fabry-Pérot configuration [43], and we measured the cantilever frequency using a phase-locked loop (see Ref. [44]).

To extract quantitative information from the MnV_2O_4 image data, we conducted a calibration experiment to characterize the magnitude and orientation of the magnetic moment of the MFM probe. A 70-nm-thick, 70-μm-long straight rectangular gold wire was patterned onto a Si substrate using electron-beam lithography and thermal evaporation. The wire measured 4 μm wide for half the length and 1 μm wide for the other half, with a steplike junction at the center (Fig. S2, Ref. [44]). We calculated the magnetic field produced by an electric current running through this simple geometry using a finite-element electromagnetic solver. For areas far from the junction, the simulation results showed near-perfect agreement with analytical calculations for an infinite wire. To ensure maximum remnant magnetization, the ambient magnetic field in the cryostat was cycled up to $B = 3$ T and back to $B = 0$ T before any measurements were performed. With a constant 5 mA current running through the wire, we recorded MFM frequency shift data in the area near the junction. Comparing these data with the calculated field curvature, we extracted the point spread function (PSF) of the MFM probe. This function is independent of the sample being scanned, and can be used to quantitatively analyze the MnV_2O_4 data because it relates the measured MFM frequency shift directly to the magnetic field curvature produced by the sample [45]. See Ref. [44] for more details.

III. RESULTS

Figure 1(a) shows MFM data collected from a region of the high-strain MnV_2O_4 sample after cooling from $T = 70$

to 40 K, well into the YK phase [33,35,50], in the presence of a weak magnetic field, $B = 3$ kG. The approximate cubic lattice directions [white arrows and text in Fig. 1(a)] were determined using room-temperature x-ray diffraction. We observe a space-filling magnetic patterning with domain and subdomain structures. Large (micrometer scale) domains of predominantly positive (blue) or negative (red) frequency shift contain and define the boundaries of 100-nm scale stripe modulations. The large domains correspond to areas of well-defined stripe direction. Additionally, the stripe pitch, amplitude, and offset vary continuously across domains, as seen in Fig. 1(d), which shows frequency shift data along the indicated line cut [yellow dashed line, Fig. 1(a)]. The pitch variation in Fig. 1(d) is only approximately 14%, but the pitch variation between the left-most and right-most domains is as large as 60%. The stripe pitch is anticorrelated between domains: in the boxed region of Fig. 1(a), the modulation pitch in the blue domain is highest and the modulation pitch in the two red domains is lowest, indicating a likely influence of mechanical strain on the magnetic patterning. By calculating the standard deviation (σ) of the frequency shift data from an entire MFM scan, we measure the degree of magnetic inhomogeneity. Figure 1(b) plots σ versus temperature for data collected during a zero-field cool of the high-strain MnV_2O_4 sample. We observe a sharp onset of magnetic inhomogeneity near $T = 58$ K and a peak at $T = 54$ K. The degree of inhomogeneity distinctly decreases between $T = 54$ and 49 K, and at $T = 49$ K, the MFM images show a clear change in the magnetic patterning. Both the raw MFM data and the derived σ versus T data clearly indicate two magnetic phase transitions in MnV_2O_4, consistent with previous reports [30,33,36,40]. Furthermore, the results shown in Fig. 1(b) are qualitatively similar to measurements of the bulk magnetization [30,33,36,40]. The correlation between bulk magnetic behavior and 0.1–10 μm scale magnetic inhomogeneity suggests that the low-temperature magnetic behavior of MnV_2O_4 can be well characterized by magnetic domain formation and heterogeneity. The observed subdomain structure explains the sharp drop in overall inhomogeneity observed below $T = 54$ K. Without a subdomain structure, we would expect the magnetic inhomogeneity to increase monotonically with decreasing temperature. These conclusions will be further explored in the discussion section.

To make a quantitative comparison between the magnitude of magnetic inhomogeneity observed in MFM and the bulk magnetic behavior reported for MnV_2O_4, we performed a calibration experiment using previously established techniques [46–49]. Further details of the calibration experiment are included in Ref. [44]. Figure 1(c) shows the instrument response of the magnetic probe extracted from measurements of the calibration sample. From top to bottom, the traces show cross sections of the PSF at locations 0, 250, 500, and 750 nm away from the probe apex. Using this measured spatial response function of the MFM probe, we quantitatively modeled the stripe pattern seen in Fig. 1(a) to yield an estimate of the local magnetization associated with the subdomain stripe features. We estimate (to within a factor of 3) the peak-to-peak magnetization associated with the stripe modulations to be $M_{pp} \approx 0.8 \times 10^5$ A/m. Because a cantilever-based magnetic probe is sensitive only to the magnetic field curvature, the absolute magnetization of a macroscopic sample cannot be determined using MFM; only gradients in the sample magnetization induce a frequency shift. Thus, our observations are consistent with two extreme possible interpretations: the stripes define regions with magnetization alternating either between $M_z = \pm M_{pp}/2$ or between $M_z = 0$ and $M_z = M_{pp}$. Magnetometry experiments on MnV_2O_4 at $T = 40$ K show that the bulk saturation magnetization is $M_z = 0.7 \times 10^5$ A/m [35], so the magnetization associated with the stripe features is comparable to the overall magnetic behavior of the sample in both extreme cases. From these results, we conclude that the highly inhomogeneous nature of the magnetic state of MnV_2O_4 represents a dominant contribution to the magnetization that must be taken into account when analyzing the low-temperature magnetic behavior of this material.

Figure 2 shows representative MFM frequency shift data collected after cooling the low-strain MnV_2O_4 sample to $T =$ 40 K in the presence of different magnetic field strengths. For fields in the range $0\,\text{kG} < B < 2.5\,\text{kG}$, we observe irregular magnetic patterning with large frequency shifts. Repeated cools with the same parameters yielded qualitatively distinct results, some with no regular patterning and others with highly regular stripe patterns. The observation that different cools yield different patterns indicates the existence of multiple, nearly degenerate metastable pattern states and the absence of significant pinning effects. Figure 2(a) shows an example of irregular patterning observed on cooling in zero applied field. In the field range $2.5\,\text{kG} < B < 7.5\,\text{kG}$, we observed 10-μm-scale domain features oriented approximately 45° relative to the cubic crystal axes. We also observed subdomain stripes that form an interwoven pattern, as can be seen in Fig. 2(b). Repeated cools in this field regime with the same parameters yielded the same domain structure, but different subdomain patterns. As the field is increased further, the number of subdomain stripes decreases until only the domain features remain [Fig. 2(c)]. Between $B = 15$ and 30 kG [Fig. 2(d)], all magnetic features are eliminated, indicating that the entire sample is a homogeneous magnetic domain.

In the context of published phase diagrams [35,50], the temperature of the above measurements should place the material well within the tetragonal/YK phase for MnV_2O_4 for the entire field range investigated. The disappearance of magnetic features between $B = 1.5$ and 30 kG is consistent with reports of a weak first-order transition associated with the realignment of tetragonal domain structure [33,50], a conclusion supported by x-ray scattering measurements [36].

Consistent with this interpretation, we identify the strong domain features in Figs. 2(b) and 2(c) as transitions between magnetic domains with magnetizations oriented parallel to different crystal axes (see Ref. [44]), mirroring previously measured structural domains [36]. As the external magnetic field is increased, tetragonal domains not oriented parallel to the external field become energetically unfavorable, resulting in the magnetic uniformity shown in Fig. 2(d).

Figure 3 shows representative MFM data collected while cooling the high-strain MnV_2O_4 sample to $T = 40$ K in the presence of different magnetic field strengths. At low fields, we again observe irregular magnetic patterning, as shown in Fig. 3(a). For fields $3\,\text{kG} < B < 7.5\,\text{kG}$, we observe a less clearly delineated domain structure, as well as single direction subdomain stripes, as shown in Fig. 3(b). Finally, for

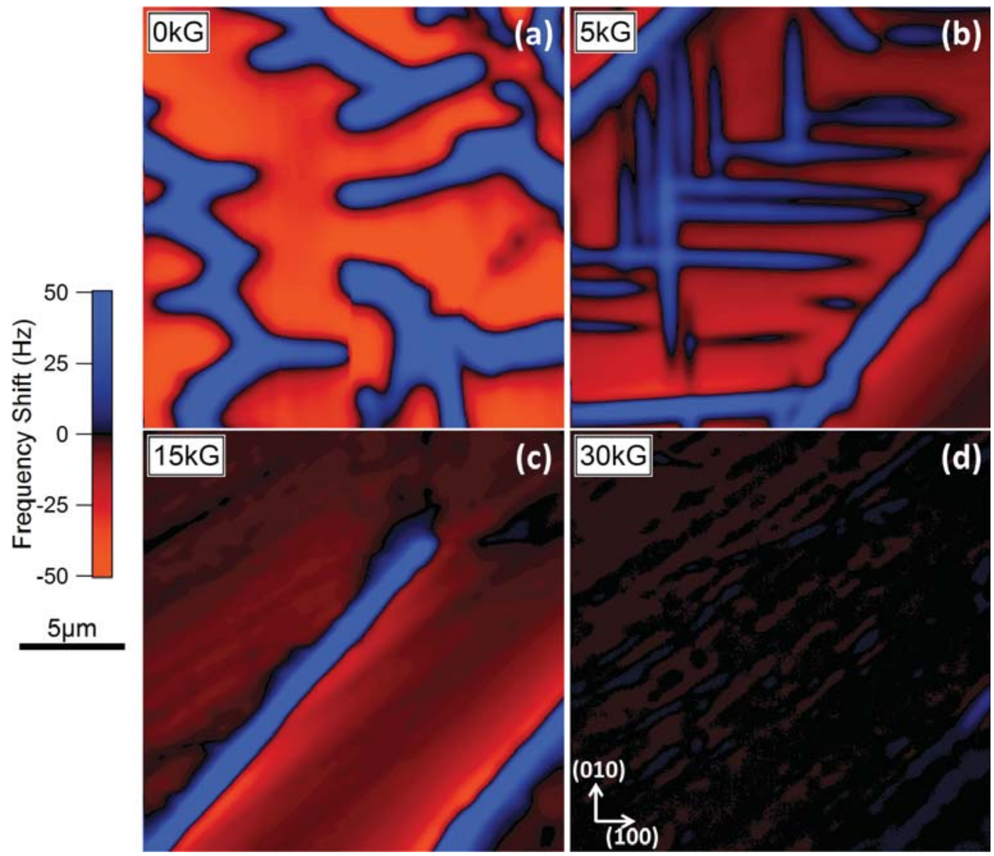

FIG. 2. MFM data of low-strain MnV_2O_4 cooled to 40 K. Images are 20 × 20 μm. The approximate cubic axes in (d) apply to all panels. (a) At low fields, the magnetic pattern is amorphous and causes large frequency shifts. In addition, we observed several distinct types of patterning during different cools at the same field value. (b) In the intermediate field regime, 10-μm-scale magnetic domains were observed. Irregular subdomain striping was observed in tweed patterns. (c) At 10 kG, subdomain striping was eliminated. (d) By 30 kG, all magnetic contrast was eliminated, indicating a single magnetic domain.

$B > 7.5$ kG [Figs. 3(c) and 3(d)], a somewhat more complex magnetic patterning develops; this patterning changes as the magnetic field is increased, and includes the development of subdomain 100-nm-scale stripe features. Figure 3(d) shows that strong magnetic inhomogeneity persists up to the highest field measured, $B = 30$ kG. Though these measurements nominally explore the same region of phase space as those in Fig. 2, the current results reveal a significant distinction between the high- and low-strain sample behaviors: high mechanical strain in the crystal lattice of MnV_2O_4 stabilizes magnetic inhomogeneity in higher magnetic fields. The distinct difference in magnetic domain patterns observed in the high-strain and low-strain samples also indicates a strong structural component to the magnetic domain pattern in MnV_2O_4. This connection could be further explored using a combination of MFM and local structural measurements, similar to that described below.

In an effort to investigate whether magnetic domain formation is observed in other Mn-based spinels exhibiting magnetoresponsive properties, we also used MFM to investigate the spatial organization of magnetic patterns in the magnetodielectric spinel, Mn_3O_4. Figure 4 is a composite MFM image of the Mn_3O_4 sample created by stitching together multiple individual MFM scans recorded in succession. The Mn_3O_4 sample was cooled in the presence of a weak magnetic field, $B = 2$ kG from above $T = 40$ to 18 K; this is well into the cell-doubled orthorhombic ferrimagnetic phase, as determined by previous measurements [34,41,52]. We observe stripe modulations very similar to those observed in MnV_2O_4. In Mn_3O_4, the stripes form a tweed pattern consisting of different regions of coordinated stripe direction. The green dashed lines in Fig. 4 indicate boundaries between the frozen-in tetragonal crystal grains, as determined by electron backscatter diffraction (EBSD). We observe a clear correspondence between the locations of tetragonal domain boundaries and the magnetic stripe region boundaries. Repeated cooling using the same parameters yields an identical set of magnetic domain boundaries, indicating that the magnetic domains are strongly pinned to the tetragonal crystal boundaries, similar to the behavior observed in the high-strain MnV_2O_4 sample. Furthermore, the size of the tetragonal domain is correlated with the stripe pitch within the domain in the Mn_3O_4 sample, with the largest tetragonal domains supporting stripes with the lowest pitch. As the tetragonal domain size shrinks, the stripe pitch increases until the MFM probe cannot resolve individual stripe features. Similar to our observations in MnV_2O_4, the tweed stripe pattern in Mn_3O_4 is eliminated by cooling in a sufficiently strong magnetic field ($B = 20$ kG). This is consistent with the observation of nearly

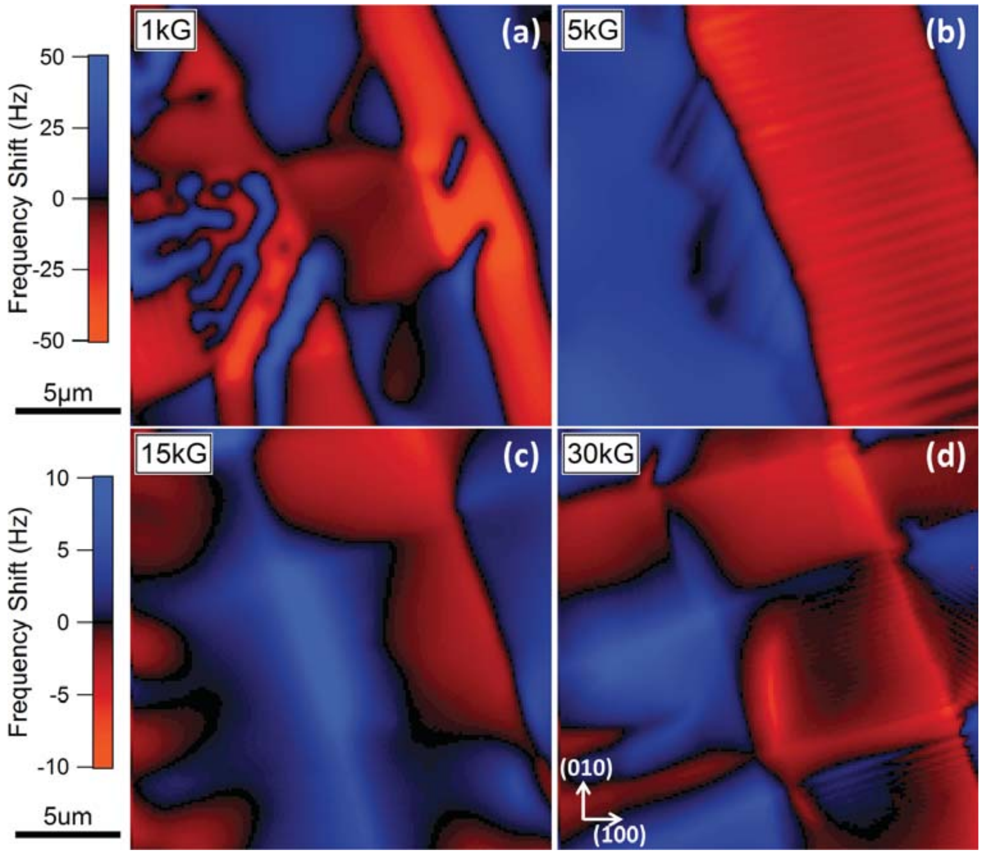

FIG. 3. MFM data of high-strain MnV_2O_4 cooled to 40 K. Images are 20×20 μm. The approximate cubic axes in (d) apply to all panels. (a) At low fields, the magnetic pattern is also amorphous (similar to the low-strain measurements) and induces large frequency shifts. (b) In the intermediate field regime, a pattern of domains and subdomain stripes appeared. No interwoven striping was observed at any field value. (c) At 15 kG, the domain pattern becomes more segmented, but retains the features seen at lower fields. Stripe modulations are still present, but are difficult to observe due to large frequency shifts between domains. (d) Strong magnetic inhomogeneity remains at $B = 30$ kG, in contrast to the low-strain sample. The stripe modulations also persist up to $B = 30$ kG.

degenerate orthorhombic phases in Mn_3O_4, and the selection of a universal orthorhombic distortion axis with applied field [34,52]. The relationship between the tetragonal domains and the magnetic pattern is further evidence of the important role that mechanical strain plays in the low-temperature magnetic stripe formation and magnetic properties of these Mn-based spinels. The presence, magnitude, and similar field behavior of magnetic inhomogeneities in both Mn_3O_4 and MnV_2O_4

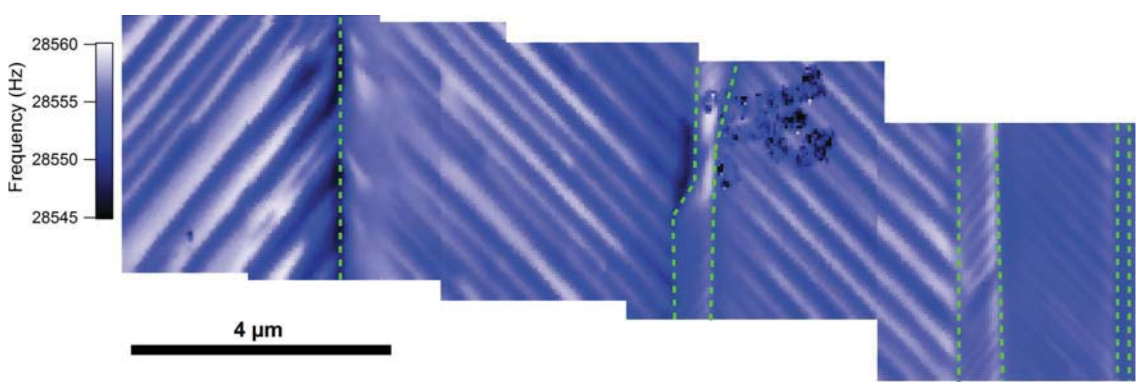

FIG. 4. Composite MFM image of Mn_3O_4 at $T = 18$ K and $B = 2$ kG. We observe tweed-pattern magnetic stripe features defined by the tetragonal crystal grain pattern (dashed green lines). The stripe widths are correlated to the domain size, suggesting a connection between the mechanical strain and the associated magnetic pattern. The patchy region in the second subpanel from the right reveals one of the location markers used to spatially register MFM data with EBSD results. The nonmagnetic marker material does not affect the magnetic behavior of the sample, but appears in the data images because of the changing topography.

indicate that such features are likely generic to a wider range of strongly spin-lattice coupled materials, particularly other magnetic spinels and magnetodielectric materials.

IV. DISCUSSION

Our investigations represent the first observations of nanoscale inhomogeneity in the low-temperature magnetic structures of bulk MnV_2O_4 and Mn_3O_4. Quantitative estimates of the magnetization associated with these nanoscale magnetic patterns indicate that the magnitude of the magnetic modulations is large, accounting for much of the bulk magnetic behavior reported in these materials. Additionally, our results show for the first time that the magnetic stripe modulations change significantly in modest magnetic field strengths that are comparable to the field strengths at which large magnetodielectric and magnetic-lattice striction effects are observed in MnV_2O_4 and Mn_3O_4 [30,36,37].

The nanoscale magnetic inhomogeneity we observe in MnV_2O_4 and Mn_3O_4 raises two fundamental questions: (i) what, if any, underlying structural inhomogeneity accompanies the magnetic inhomogeneity; (ii) to what extent does the magnetic inhomogeneity contribute to the magnetoresponsive phenomena observed in MnV_2O_4 and Mn_3O_4 [16–18]?

Addressing the first issue, substantial direct and indirect evidence indicates that the nanoscale magnetic inhomogeneity we observe at low temperatures in MnV_2O_4 and Mn_3O_4 is associated with an underlying structural modulation. Bulk x-ray diffraction measurements on polycrystalline Mn_3O_4 [51] show evidence for a mixture of tetragonal and orthorhombic phases, and the coexistence of tetragonal (paramagnetic) and orthorhombic phases at low temperatures in Mn_3O_4 is also supported by recent muon spin resonance measurements of single-crystal Mn_3O_4, which reveal a mixture of magnetically ordered and disordered volumes at low temperatures [21]. The phonon and magnon Raman scattering spectra of heavily twinned samples of Mn_3O_4 also show evidence for phase coexistence at low temperatures, which may include coexisting orthorhombic and tetragonal phases [38]. More recent Raman experiments of the phonon and magnon spectra of untwinned Mn_3O_4 samples show clear evidence for coexisting face-centered orthorhombic and cell-doubled orthorhombic phases at low temperatures [52], consistent with the presence of a mesoscale structural modulation in this material. In MnV_2O_4, TEM measurements revealed the coexistence of tetragonal twinning domains with different c-axis orientations [42], and the sensitivity to strain we observe in our measurements of MnV_2O_4 support the conclusion that the nanoscale magnetic modulation we observe in this material is associated with an underlying structural modulation. Altogether, these results provide strong evidence that the magnetic modulations observed with MFM in both MnV_2O_4 and Mn_3O_4 are associated with an underlying structural modulation that betrays the strong coupling of spin, orbital, and structural degrees of freedom in these materials [36,37].

Notably, mesoscale magnetostructural modulations have been observed in other magnetic materials exhibiting strong spin-lattice coupling, including $La_{1.99}Sr_{0.01}CuO_4$ [53], $Co_{0.5}Ni_{0.205}Ga_{0.295}$ [54], and the Mn-doped spinel $CoFe_2O_4$ [55]. Mesoscale magnetostructural pattern formation in materials has been explained using Landau expansions of the elastic energy in powers of the strain and the strain gradients [54,56–59], and several key conditions for the formation of mesoscale magnetostructural modulations near structural phase transitions of strongly spin-lattice coupled materials have been delineated [54,60]: (i) a sensitivity of the system to local symmetry-breaking perturbations, e.g., Jahn-Teller instabilities; (ii) the presence of long-range interactions, such as magnetic interactions, that can stabilize particular structural phases locally; and (iii) some local anisotropy, e.g., a surface, defect, or grain boundary, to determine the specific modulation pattern. All of these essential ingredients for the nucleation of mesoscale magnetostructural domain regions are present in both MnV_2O_4 and Mn_3O_4. It is also worth noting that both MnV_2O_4 and Mn_3O_4 have orbitally active octahedral (B) sites (V^{3+} in MnV_2O_4 and Mn^{3+} in Mn_3O_4), which has been shown to favor an instability toward spinodal decomposition into coexisting structural phases [61], consistent with our evidence for coexisting tetragonal and orthorhombic phases in Mn_3O_4 and similar to earlier evidence for phase coexistence in the Mn-doped spinel $CoFe_2O_4$ [55].

The newest and most significant demonstration from this MFM study is that the mesoscale magnetic domain patterns observed in MnV_2O_4 and Mn_3O_4 are readily controlled with modest magnetic fields; indeed, the magnetic field strengths at which we observe the magnetic stripe modulations to change in both in MnV_2O_4 and Mn_3O_4 correspond closely to the magnetic field values at which magnetodielectric effects and magnet-field-tuned lattice striction effects are observed in both MnV_2O_4 [30,37] and Mn_3O_4 [30,36]. This close correspondence offers strong evidence that the magnetically responsive properties of MnV_2O_4 and Mn_3O_4 are not associated with homogeneous properties of these materials, but are rather associated with the materials' intrinsic magnetic inhomogeneities, which are ultimately driven by the competition between long-range magnetic interactions and strain energies. Significantly, the presence of domain walls and mesoscale phase separation has been shown to be instrumental in lowering the energy barrier for field-induced phase changes in complex materials [28,29], and indeed, we propose that the mesoscale magnetostructural patterns evident in our MFM results—and their strong susceptibility to magnetic-field manipulation—are primarily responsible for the large magnetic susceptibilities observed in MnV_2O_4 [30,37] and Mn_3O_4 [30,36].

V. CONCLUSIONS

We employed cryogenic MFM and room-temperature EBSD to investigate the nanoscale magnetic properties of the two multiferroic spinel materials MnV_2O_4 and Mn_3O_4. Our MFM measurements reveal significant nanoscale magnetic domain formation that has been overlooked by previous bulk probe studies. The magnitude of the magnetic modulations in these materials are comparable to the bulk magnetizations measured in these materials, and consequently this nanoscale magnetic inhomogeneity cannot be neglected when considering the overall magnetic behavior of the two materials. The magnetic patterning cannot be attributed solely to simple magnetic domain formation. Theoretical proposals and data interpretations for MnV_2O_4 and Mn_3O_4 that rely on assumptions of magnetic homogeneity must be revisited. In addition, the presence of nanoscale magnetic inhomogeneity in these two related compounds suggests this phenomenon may be present in other multiferroic spinels.

We have established that mechanical strain plays an important role in the phenomenology of the low-temperature magnetic patterning. In Mn_3O_4, the tweed stripe pattern is defined by the tetragonal crystal grains, and stripe pitch is correlated to grain size. In MnV_2O_4, the interwoven stripe pattern is also defined by the tetragonal domain structure. When the tetragonal domain structure is determined at experimentally accessible temperatures, we can control the magnetic patterning through application of an external magnetic field. Inducing mechanical strain in MnV_2O_4 produces a more complex magnetic pattern at intermediate magnetic fields, and stabilizes magnetic inhomogeneity at higher magnetic fields. These findings are consistent with theoretical results showing that mesoscale magnetic inhomogeneity can significantly lower the energy barrier for strain- and field-dependent phase changes in complex materials, and offers strong evidence that magnetic domain formation plays an important role in the magnetoresponsive behavior of these spinel materials.

ACKNOWLEDGMENTS

Research was supported by the US Department of Energy under Award No. DE-FG02-07ER46453 (B.W., X.W., T.N., and R.B.), and by the National Science Foundation under Grants NSF DMR 1464090 and NSF DMR 1800982 (S.L.G. and S.L.C.) and NSF DMR 1455264 (G.J.M.). Research at the National High Magnetic Field Laboratory was supported by the National Science Foundation under Grant No. DMR-1157490, and by the state of Florida. The work was carried out in part in the Frederick Seitz Materials Research Laboratory Central Research Facilities, University of Illinois.

[1] C.-W. Nan, M. I. Bichurin, S. Dong, D. Viehland, and G. Srinivasan, Multiferroic magnetoelectric composites: Historical perspective, status, and future directions, J. Appl. Phys. **103**, 031101 (2008).

[2] H. Katsura, N. Nagaosa, and A. V. Balatsky, Spin Current and Magnetoelectric Effect in Noncollinear Magnets, Phys. Rev. Lett. **95**, 057205 (2005).

[3] D. I. Khomskii, Multiferroics: Different ways to combine magnetism and ferroelectricity, J. Magn. Magn. Mater. **306**, 1 (2006).

[4] S.-W. Cheong and M. Mostovoy, Multiferroics: A magnetic twist for ferroelectricity, Nat. Mater. **6**, 13 (2007).

[5] S. Yang, H. X. Bao, D. Z. Xue, C. Zhou, J. H. Gao, Y. Wang, J. Q. Wang, X. P. Song, Z. B. Sun, X. B. Ren, and K. Otsuka, Magnetodielectric effect from the onset of ferrimagnetic transition in $CoCr_2O_4$, J. Phys. D **45**, 265001 (2012).

[6] E. K. H. Salje, Multiferroic domain boundaries as active memory devices: Trajectories towards domain boundary engineering, Chem. Phys. Chem. **11**, 940 (2010).

[7] E. K. H. Salje, O. Aktas, M. A. Carpenter, V. V. Laguta, and J. F. Scott, Domains Within Domains and Walls Within Walls: Evidence for Polar Domains in Cryogenic $SrTiO_3$, Phys. Rev. Lett. **111**, 247603 (2013).

[8] G. Lawes, A. P. Ramirez, C. M. Varma, and M. A. Subramanian, Magnetodielectric Effects from Spin Fluctuations in Isostructural Ferrimagnetic and Antiferromagnetic Systems, Phys. Rev. Lett. **91**, 257208 (2003).

[9] C.-H. Yang, T. Y. Koo, and Y. H. Jeong, How to obtain magnetocapacitance effects at room temperature: The case of Mn-doped $BiFeO_3$, Solid State Commun. **134**, 299 (2005).

[10] T. Katsufuji and H. Takagi, Coupling between magnetism and dielectric properties in the quantum paraelectric $EuTiO_3$, Phys. Rev. B **64**, 054415 (2001).

[11] U. Adem, G. Nenert, Arramel, N. Mufti, G. R. Blake, and T. T. M. Palstra, Magnetodielectric coupling by exchange striction in $Y_2Cu_2O_5$, Eur. Phys. J. B **71**, 393 (2009).

[12] U. Adem, M. Mostovoy, N. Bellido, A. A. Nugroho, C. Simon, and T. T. M. Palstra, Scaling behavior of the magnetocapacitance of $YbMnO_3$, J. Phys.: Condens. Matter **21**, 496002 (2009).

[13] N. Mufti, G. R. Blake, and T. T. M. Palstra, Magnetodielectric coupling in $MnCr_2O_4$ spinel, J. Magn. Magn. Mater. **321**, 1767 (2009).

[14] T. Suzuki, K. Adachi, and T. Katsufuji, Coupling between magnetic, dielectric properties and crystal structure in MnT_2O_4 (T = V,Cr,Mn), J. Phys.: Conf. Ser. **31**, 235 (2006).

[15] X. Luo, W. J. Lu, Z. H. Huang, X. B. Hu, L. Hu, X. B. Zhu, Z. R. Yang, W. H. Song, J. M. Dai, and Y.P. Sun, Large reversible magnetocaloric effect in spinel MnV_2O_4 with minimal Al substitution, J. Magn. Magn. Mater. **324**, 766 (2012).

[16] M. Kim, X. M. Chen, Y. I. Joe, E. Fradkin, P. Abbamonte, and S. L. Cooper, Mapping the Magneto-Structural Quantum Phases of Mn_3O_4, Phys. Rev. Lett. **104**, 136402 (2010).

[17] R. Tackett, G. Lawes, B. C. Melot, M. Grossman, E. S. Toberer, and R. Seshadri, Magnetodielectric coupling in Mn_3O_4, Phys. Rev. B **76**, 024409 (2007).

[18] T. Suzuki and T. Katsufuji, Magnetodielectric properties of spin-orbital coupled Mn_3O_4, Phys. Rev. B **77**, 220402(R) (2008).

[19] G. J. MacDougall, I. Brodsky, A. A. Aczel, V. O. Garlea, G. E. Granroth, A. D. Christianson, T. Hong, H. D. Zhou, and S. E. Nagler, Magnons and a two-component spin gap in FeV_2O_4, Phys. Rev. B **89**, 224404 (2014).

[20] S. Lee, H. Takagi, D. Louca, M. Matsuda, S. Ji, H. Ueda, Y. Ueda, T. Katsufuji, J.-H. Chung, S. Park, S.-W. Cheong, and C. Broholm, Frustrated magnetism and cooperative phase transitions in spinels, J. Phys. Soc. Jpn. **79**, 011004 (2010).

[21] G. J. MacDougall *et al.*, Observation and control of domain wall order in Mn_3O_4 (unpublished).

[22] K. A. Gschneidner Jr., V. K. Pecharsky, and A.O. Tsokol, Recent developments in magnetocaloric materials, Rep. Prog. Phys. **68**, 1479 (2005).

[23] G. Giovannetti, A. Stroppa, S. Picozzi, D. Baldomir, V. Pardo, S. Blanco-Canosa, F. Rivadulla, S. Jodlauk, D. Niermann, J. Rohrkamp, T. Lorenz, S. Streltsov, D. I. Khomskii, and J. Hemberger, Dielectric properties and magnetostriction of the collinear multiferroic spinel CdV_2O_4, Phys. Rev. B **83**, 060402(R) (2011).

[24] M. Onoda and J. Hasegawa, A distortion of pseudotetramers coupled with the Jahn-Teller effect in the geometrically

frustrated spinel system CdV_2O_4, J. Phys.: Condens. Matter **15**, L95 (2003).
[25] P. G. Radaelli, Orbital ordering in transition metal spinels, New J. Phys. **7**, 53 (2005).
[26] Z. Y. Tian, P. M. Loutou, N. Bahlawane, and P. H. T. Ngamou, Synthesis of the catalytically active Mn_3O_4 spinel and its thermal properties, J. Phys. Chem. C **117**, 6218 (2013).
[27] H. Xia, Y. Wan, F. Yan, and L. Lu, Manganese oxide thin films prepared by pulsed laser deposition for thin film microbatteries, Mater. Chem. Phys. **143**, 720 (2014).
[28] K. H. Ahn, T. F. Seman, T. Lookman, and A. R. Bishop, Role of complex energy landscapes and strains in multiscale inhomogeneities in perovskite manganites, Phys. Rev. B **88**, 144415 (2013).
[29] K. H. Ahn, T. Lookman, and A. R. Bishop, Strain-induced metalinsulator phase coexistence in perovskite manganites, Nature (London) **428**, 401 (2004).
[30] J.-H. Chung, J.-H. Kim, S.-H. Lee, T. J. Sato, T. Suzuki, M. Katsumura, and T. Katsufuji, Magnetic excitations and orbital physics in the ferrimagnetic spinels MnB_2O_4 (B = Mn, V), Phys. Rev. B **77**, 054412 (2008).
[31] G. B. Jensen and O. V. Nielsen, The magnetic structure of Mn_3O_4 Hausmannite between 4.7 K and Neel point, 41 K, J. Phys. C **7**, 409 (1974).
[32] B. Chardon and F. Vigneron, Mn_3O_4 commensurate and incommensurate magnetic structures, J. Magn. Magn. Mater. **58**128 (1986).
[33] H. D. Zhou, J. Lu, and C. R. Wiebe, Spin ordering and orbital ordering transitions in MnV_2O_4, Phys. Rev. B **76**, 174403 (2007).
[34] Y. Nii, H. Sagayama, H. Umetsu, N. Abe, K. Taniguchi, and T. Arima, Interplay among spin, orbital, and lattice degrees of freedom in a frustrated spinel Mn_3O_4, Phys. Rev. B **87**, 195115 (2013).
[35] V. Hardy, Y. Breard, and C. Martin, Phase diagram of the spinel oxide MnV_2O_4, Phys. Rev. B **78**, 024406 (2008).
[36] T. Suzuki, M. Katsumura, K. Taniguchi, T. Arima, and T. Katsufuji, Orbital Ordering and Magnetic Field Effect in MnV_2O_4, Phys. Rev. Lett. **98**, 127203 (2007).
[37] K. Adachi, T. Suzuki, K. Kato, K. Osaka, M. Takata, and T. Katsufuji, Magnetic-Field Switching of Crystal Structure in an Orbital-Spin-Coupled System: MnV_2O_4, Phys. Rev. Lett. **95**, 197202 (2005).
[38] S. L. Gleason, T. Byrum, Y. Gim, A. Thaler, P. Abbamonte, G. J. MacDougall, L. W. Martin, H. D. Zhou, and S. L. Cooper, Magnon spectra and strong spin-lattice coupling in magnetically frustrated MnB_2O_4 (B = Mn, V): Inelastic light-scattering studies, Phys. Rev. B **89**, 134402 (2014).
[39] K. Takubo, R. Kubota, T. Suzuki, T. Kanzaki, S. Miyahara, N. Furukawa, and T. Katsufuji, Evolution of phonon Raman spectra with orbital ordering in spinel MnV_2O_4, Phys. Rev. B **84**, 094406 (2011).
[40] V. O. Garlea, R. Jin, D. Mandrus, B. Roessli, Q. Huang, M. Miller, A. J. Schultz, and S. E. Nagler, Magnetic and Orbital Ordering in the Spinel MnV_2O_4, Phys. Rev. Lett. **100**, 066404 (2008).
[41] M. Kim, X. M. Chen, X. Wang, C. S. Nelson, R. Budakian, P. Abbamonte, and S. L. Cooper, Pressure and field tuning the magnetostructural phases of Mn_3O_4: Raman scattering and x-ray diffraction studies, Phys. Rev. B **84**, 174424 (2011).
[42] Y. Murakami, T. Suzuki, Y. Nii, S. Murai, T. Arima, R. Kainuma, and D. Shindo, Application of strain to orbital-spin-coupled system MnV2O4 at cryogenic temperatures within a transmission electron microscope, Microscopy **65**, 223 (2016); Y. Murakami, Y. Nii, T. Arima, D. Shindo, K. Yanagisawa, and A. Tonomura, Magnetic domain structure in the orbital-spin-coupled system MnV2O4, Phys. Rev. B **84**, 054421 (2011).
[43] T. Fukuma, M. Kimura, K. Kobayashi, K. Matsushige, and H. Yamada, Development of low noise cantilever deflection sensor for multienvironment frequency-modulation atomic force microscopy, Rev. Sci. Instrum. **76**, 053704 (2005).
[44] See Supplemental Material at http://link.aps.org/supplemental/10.1103/PhysRevMaterials.2.064407 for further information on the design of the magnetic probes used for the current experiments and calibration of resultant data.
[45] P. J. Rous, R. Yongsunthon, A. Stanishevsky, and E. D. Williams, Real-space imaging of current distributions at the submicron scale using magnetic force microscopy: Inversion methodology, J. Appl. Phys. **95**, 2477 (2004).
[46] J. Lohau, S. Kirsch, A. Carl, G. Dumpich, and E. F. Wasserman, Quantitative determination of effective dipole and monopole moments of magnetic force microscopy tips, J. Appl. Phys. **86**, 3410 (1999).
[47] T. Goddenhenrich, H. Lemke, M. Muck, U. Hartmann, and C. Heiden, Probe calibration in magnetic force microscopy, Appl. Phys. Lett. **57**, 2612 (1990).
[48] K. L. Babcock, V. B. Elings, J. Shi, D. D. Awshalom, and M. Dugas, Field-dependence of microscopic probes in magnetic force microscopy, Appl. Phys. Lett. **69**, 705 (1996).
[49] L. Kong and S. Y. Chou, Quantification of magnetic force microscopy using a micronscale current ring, Appl. Phys. Lett. **70**, 2043 (1997).
[50] K. Myung-Whun, J. S. Kim, T. Katsufuji, and R. K. Kremer, Magnetic susceptibility and specific heat of a spinel MnV_2O_4 single crystal, Phys. Rev. B **83**, 024403 (2011).
[51] M. C. Kemei, J. K. Harada, R. Seshadri, and M. R. Suchomel, Structural Change and Phase Coexistence Upon Magnetic Ordering in the Magnetodielectric Spinel Mn_3O_4, Phys. Rev. B **90**, 064418 (2014).
[52] T. Byrum, S. L. Gleason, A. Thaler, G. J. MacDougall, and S. L. Cooper, Effects of magnetic field and twinned domains on magnetostructural phase mixture in Mn_3O_4: Raman scattering studies of untwinned crystals, Phys. Rev. B **93**, 184418 (2016).
[53] A. Lavrov, S. Komiya, and Y. Ando, Magnetic shape-memory effects in a crystal, Nature (London) **421**, 230 (2003).
[54] A. Saxena, T. Cast´an, A. Planes, M. Porta, Y. Kishi, T. A. Lograsso, D. Viehland, M. Wuttig, and M. De Graef, Origin of Magnetic and Magnetoelastic Tweedlike Precursor Modulations in Ferroic Materials, Phys. Rev. Lett. **92**, 197203 (2004).
[55] C. L. Zhang, C. M. Tseng, C. H. Chen, S. Yeo, Y. J. Choi, and S.-W. Cheong, Magnetic nanocheckerboards with tunable sizes in the Mn-doped $CoFe_2O_4$ spinel, Appl. Phys. Lett. **91**, 233110 (2007).
[56] A. M. Bratkovsky, S. C.Marais, V. Heine, and E. K. H. Salje, The theory of fluctuations and texture embryos in structural phase transitions mediated by strain, J. Phys.: Condens. Matter **6**, 3679 (1994).
[57] A. M. Bratkovsky, E. K. Salje, S. C. Marais, and V. Heine, Strain coupling as the dominant interaction in structural phase transitions, Phase Transitions **55**, 79 (1995).

[58] A. E. Jacobs, Landau theory of a constrained ferroelastic in two dimensions, Phys. Rev. B **52**, 6327 (1995).
[59] A. E. Jacobs, Landau theory of structures in tetragonal-orthorhombic ferroelastics, Phys. Rev. B **61**, 6587 (2000).
[60] X. Wang, Imaging magnetic order in magnetostructural phases of Mn_3O_4, PhD thesis, University of Illinois, 2012.
[61] M. A. Ivanov, N. K. Tkachev, and A. Y. Fishman, Phase transformations of the decomposition type in systems with orbital degeneracy, Low Temp. Phys. **28**, 613 (2002).